Modulation Recognition of BPSK/QPSK Signals based on Features in the Graph Domain

Li Yang[1], Guobing Hu[1*], Xiaoyang Xu[2], and Pinjiao Zhao[1]
[1] College of Electronic and Information Engineering, Jinling Institute of Technology
Nanjing, 211169 China
[e-mail: s0304152@jit.edu.cn]
[2] College of Network Communication Engineering, Jinling Institute of Technology
Nanjing, 211169 China
[e-mail: xuyang@jit.edu.cn]
[*]Corresponding author: Guobing Hu

Received June 18, 2022; revised August 17, 2022; accepted October 28, 2022; published November 30, 2022

Abstract

The performance of existing recognition algorithms for binary phase shift keying (BPSK) and quadrature phase shift keying (QPSK) signals degrade under conditions of low signal-to-noise ratios (SNR). Hence, a novel recognition algorithm based on features in the graph domain is proposed in this study. First, the power spectrum of the squared candidate signal is truncated by a rectangular window. Thereafter, the graph representation of the truncated spectrum is obtained via normalization, quantization, and edge construction. Based on the analysis of the connectivity difference of the graphs under different hypotheses, the sum of degree (SD) of the graphs is utilized as a discriminate feature to classify BPSK and QPSK signals. Moreover, we prove that the SD is a Schur-concave function with respect to the probability vector of the vertices (PVV). Extensive simulations confirm the effectiveness of the proposed algorithm, and its superiority to the listed model-driven-based (MDB) algorithms in terms of recognition performance under low SNRs and computational complexity. As it is confirmed that the proposed method reduces the computational complexity of existing graph-based algorithms, it can be applied in modulation recognition of radar or communication signals in real-time processing, and does not require any prior knowledge about the training sets, channel coefficients, or noise power.

Keywords: Graph representation, Modulation recognition, Majorization inequality, Phase modulation signal, Schur concavity

http://doi.org/10.3837/tiis.2022.11.016 **ISSN : 1976-7277**

1. Introduction

In digital receivers, modulation recognition of radar or communication signals is an indispensable intermediate link between signal detection and demodulation. Modulation recognition is extensively used in both military and civilian fields [1, 2]. In military applications, such as electronic reconnaissance, modulation recognition is a critical prerequisite for obtaining parameters of the enemy radars; whereas in civil applications, such as cognitive radio, modulation recognition is one of the key tasks in spectrum sensing. Moreover, in intelligent communication systems based on 5G/6G technology, modulation recognition is an indispensable step in facilitating the assistance of artificial intelligence (AI) [3].

Existing modulation recognition algorithms can be divided into two categories: likelihood-based (LB) and feature-based (FB) algorithms [1]. LB algorithms require a prior information of the signals and channel coefficients, and can attain optimal performance in the Bayesian sense. However, their computational complexity is relatively high. In practice, LB algorithms cannot be realized when the signal parameter space is complex. By contrast, the FB algorithm, which depends on the mechanism of feature engineering, has relatively lower computational complexity. The FB algorithm can be further divided into two sub-classes: data-driven-based (DDB) [4-6] and model-driven-based (MDB) [7] algorithms. Generally, the feature engineering mechanism of DDB is based on machine learning or deep learning frameworks [8-10], and it depends on vast labeled training samples. However, in non-cooperative contexts, such as electronic reconnaissance, it is difficult to obtain training samples. Moreover, another problem encountered by DDB algorithms is that accurate estimation and matching of SNR will cause computational fatigue and difficulty in training. The modulation recognition algorithms based on MDB feature engineering include the following: time-frequency analysis [11], higher order cumulant [12], distribution fitting test [13], and cyclostationarity test [7]. However, most of them depend on time series analysis framework.

Recently, a novel graph-based signal processing tool for time series signals was proposed. Accordingly, graph-based signal detection and modulation recognition were initially investigated in [14, 15]. Those algorithms aimed to transform a time series, such as the samples in the time or frequency domains, to a graph with several vertices points and edges, and then extract graph features to detect [14] or recognize signals [16]. From the perspective of feature engineering, graph-based modulation recognition algorithms can be divided into two categories: machine learning-based algorithm and features-based algorithm. In [17], a graph-based modulation recognition algorithm based on Kullback–Leibler divergence was proposed. The features were defined using the elements in the adjacency matrix of the graph, and optimized by feature selection to decrease redundancy. In [16, 18], the fractional low-order cyclic spectrum and generalized second-order cyclic spectrum of the received signals under α-stable noise were utilized as the inputs fed into the signal-to-graph convertor (SGC), respectively; the features of the constructed graph were extracted based on their adjacency matrices. Accordingly, classifications were performed by checking the distance between the features extracted from the training sets and those extracted from the testing sets. However, the aforementioned approaches severely rely on a large amount of labeled training samples.

Another category of recognition algorithms based on the completeness of graphs has been proposed. In [19], nonlinear transform of the spectra of phase modulation signals, i.e., the quadratic spectra and fourth power spectra were selected as the inputs fed to the SGC. Subsequently, recognition was performed by detecting the completeness of the graph. Inspired by [19], it is easy to formulate BPSK/QPSK modulation identification based on checking the

completeness of the graph generated from the modified power spectrum of candidate signals. The modified power spectrum can be obtained by eliminating several large magnitude lines in the spectrum of the squared signal. In particular, the order of computational complexity of those algorithms is of $O(N^2)$, where N denotes the length of the samples. The computational costs increase significantly even with a moderate sample size, which is unfavorable to real-time processing applications. Moreover, the performance of graph-based algorithms degrade under low SNRs. Hence, it is vital to investigate the novel signal representation framework and develop a new signal modulation recognition algorithm.

In this study, to improve the performance under low SNRs and reduce the computational complexity of existing graph-based algorithms, we propose a BPSK/QPSK signal modulation recognition algorithm based on the feature, i.e., sum of degree (SD). First, the truncated power spectrum of signal squaration (SS) was transformed to a graph, and then the SD of the graph was extracted as a feature to classify BPSK and QPSK signals. Based on the simulation results, the proposed algorithm performs well under low SNRs, and has better preferable behavior in terms of computational complexity and robustness, compared with existing graph-based algorithms. Moreover, the proposed algorithm can function effectively without any prior knowledge about the training sets, channel coefficients, or noise power.

The innovative contributions of this study are as follows:

1) Based on the majorization inequality theory, we prove that the average SD of a graph is a Schur–concave function of the probability vector of the vertex (PVV). The PVV represents the distribution of a quantized samples on each vertex. Accordingly, the connectivity of the graph that transformed from random sample sequences can be explained by comparing the majorization relationships between different random sequences distributions.

2) We introduce an efficient BPSK/QPSK recognition algorithm using the SD features of the graphs. The sample size of the random signal fed to the SGC is decreased by truncation, which reduces the computational cost. Moreover, the SD feature is robust to the influence of truncation; thus, yielding outstanding performance under low SNRs.

3) Extensive simulations are conducted to evaluate the effectiveness of the proposed algorithm. Additionally, compared with existing graphed-based algorithms, the proposed algorithm exhibits superior performance in balancing computational complexity and recognition performance under low SNRs.

The remainder of this article is organized as follows. Signal mode and the basis of the graph transformation is described in Section Ⅱ. The proposed algorithm based on SD is presented in Section Ⅲ, and the simulation results are presented in Section Ⅳ. Finally, conclusions are drawn in Section Ⅴ.

2. BACKGROUND

2.1 Signal mode

The model of the candidate signals can be expressed by

$$x(n) = s_i(n) + w(n) = A\exp(j[2\pi f_0 n\Delta t + \pi d_i(n) + \theta]) + w(n), 0 \le n \le N-1, i = 0,1, \quad (1)$$

where $s_0(n)$ represents the BPSK signal, $s_1(n)$ represents the QPSK signal, $d_i(n)$ denotes the phase encoding functions of the signals, i.e., $d_0(n) = \{0,1\}$ for BPSK, and $d_1(n) = \{0,1,2,3\}$ for QPSK. A indicates the amplitude, N indicates the sample size, f_0 denotes the carrier

frequency, Δt symbolizes the sampling interval, θ signifies the initial phase, and $w(n)$ represents complex additive white Gaussian noise (AWGN) with zero mean and a variance of $2\sigma_0^2$; it is uncorrelated to the signal $s_i(n)$.

The identification of the modulation mode of BPSK/QPSK signals can be formulated via the following binary hypothesis test:

H_0: The candidate signal is BPSK.

H_1: The candidate signal is QPSK.

2.2 Basic of SGC

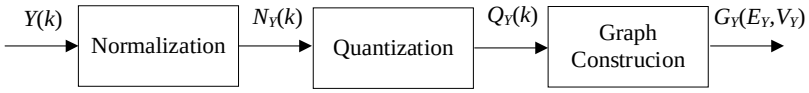

Fig. 1. Framework of SGC.

As shown in **Fig. 1**, the transformation of a random sequence $Y(k)$ to a graph $G_Y(E_Y, V_Y)$ can be divided into three steps: normalization, quantization, and graph construction [15]. Notably, the random sequence can be expressed in the original time domain signal or other transformation domains. Details of the three steps are as follows.

Step 1: Normalization. The random sequence $Y(k)$ is normalized in the range [0,1], and can be expressed as

$$N_Y(k) = \frac{Y(k) - Y_{\min}(k)}{Y_{\max}(k) - Y_{\min}(k)}, k = 0,1,...,N\text{-}1, \tag{2}$$

where $Y_{\max}(k)$ and $Y_{\min}(k)$ represent the maximum and minimum values of $Y(k)$, respectively.

Step 2: Quantization. For a given quantization level N_0, $N_Y(k)$ can be uniformly quantized by,

$$Q_Y(k) = i + 1, \tag{3}$$

if $i/N_0 \le N_Y(k) < (i+1)/N_0, 0 \le i \le N_0 - 1$ for $k = 0,1,...,N-1$.

Step 3: Graph construction. A graph $G_Y = \{E_Y, V_Y\}$ can be constructed from $Q_Y(k)$, where $V_Y = \{v_1, v_2, ...v_q\}$ represents the vertices set and $E_Y = \{e_{\alpha,\beta} \mid v_\alpha \in V_Y, v_\beta \in V_Y\}$ represents the edges. The detailed scheme is as follows: trace the amplitude transitions from $Q_Y(k)$ to $Q_Y(k+1)$; two vertices are connected when there is a level jumping between v_α and v_β, i.e., $e_{\alpha,\beta} = 1$; otherwise, the two vertices are not connected, i.e., $e_{\alpha,\beta} = 0$.

Following that, two crucial terms involved in transforming modulation signals to graphs are given below.

Definition 1. PVV: For an independently identically distributed (i.i.d.) random sequence $Y \sim f_Y(y)$, which is transformed to a graph by SGC. The number of vertices of the graph is given by N_0. Here, PVV is defined as $\mathbf{p} = (p_1, p_2, ..., p_{N_0})^T$, where

$$p_i = I_i(G_Y)/N, i = 1,2...,N_0 \tag{4}$$

where $I_i(G_Y)$ represents the total number of quantized samples located in the ith vertex on graph G_Y, and N indicates the sample size of random sequence $Y(k)$.

Definition 2. Partial sum of PVV: Let

$$S_{p_\Omega} = \sum_{i=1}^{\Omega} p_{[i]}, 1 \le i \le \Omega \le N_0, \tag{5}$$

as the partial sum of PVV, i.e., $\mathbf{p}$, considering the former Ω items, where $p_{[i]}$ denotes the decreasing rearrangements of the PVV, i.e., $\mathbf{p}_\downarrow = (p_{[0]}, p_{[1]},..., p_{[N_0]})^T$.

According to Definitions 1 and 2, under the H_0 assumption, the PVV is denoted by $\mathbf{p}$, and the partial sum is $S_{p_\Omega} = \sum_{i=1}^{\Omega} p_{[i]}, 1 \le i \le \Omega \le N_0$. However, under the H_1 assumption, the PVV is set as $\mathbf{q}$, and the partial sum items is $S_{q_\Omega} = \sum_{j=1}^{\Omega} q_{[j]}, 1 \le j \le \Omega \le N_0$. The partial sum of PVV can be used to compare the randomness of the probability vectors [20], that is, if $S_{p_\Omega} > S_{q_\Omega}$, it follows that

$$\mathbf{q} \prec \mathbf{p}, \tag{6}$$

indicating that $\mathbf{q}$ is majorized by $\mathbf{p}$, implying that $\mathbf{q}$ is more random than $\mathbf{p}$.

According to [14], for a particular distributed random sequence, its probability distribution and PVV determine the connectivity of the graph, and also partly determines the probability of the random sequences being transformed to a complete graph.

3. PROPOSED ALGORITHM

In this section, we first analyze the factors that degrade the performance and increase the computational complexity of existing graph-based modulation recognition algorithms [15, 19]. Consequently, a novel algorithm based on SD is presented, which has a better performance in low SNR and a lower computational complexity. The key adjustments include: 1) the input fed to the SGC is the truncated SS (TSS) other than SS itself. 2) the feature extracted to discriminate the modulation signals is the SD of the graph. Indeed, truncation can reduce the input sample size of SGC, thereby reducing the processing complexity of the graph conversion. Moreover, extracting the SD feature relies on linear operation; hence, it avoids eigen decomposition of the Laplacian matrix of the graph, thereby reducing the computational complexity further. In addition, the SD feature can also improve the recognition performance owing to its robustness and excellent discriminability. A diagram that summarizes this algorithm is shown in **Fig. 2**.

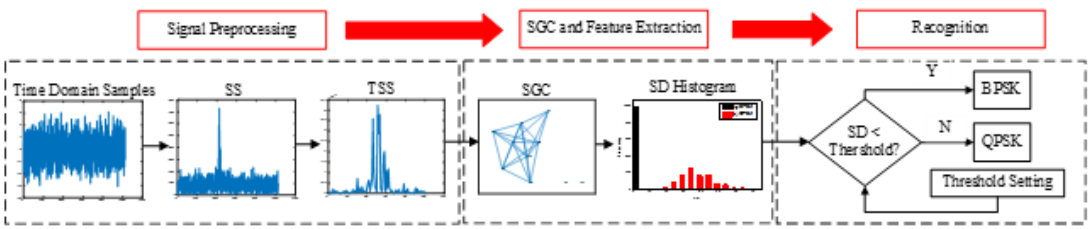

Fig. 2. Framework of the proposed algorithm.

3.1 Conventional graphs-based modulation recognition algorithm

Existing graph-based modulation recognition algorithms rely on the detection of the completeness of the graph [15, 19], where the modified spectrum of squared signal (MSS) is utilized as an input fed to the SGC. In the MSS, about 3~5 spectrum lines around the maximum of the SS are set to zero. Accordingly, the SNRs of the input fed to the SGC significantly decreases owing to the modification, resulting in energy loss and performance deterioration. In addition, the sample size of the input signal for SGC mainly decides its computational complexity. The main computational complexities of SGC are roughly listed in **Table 1**.

Table 1. Main computational complexity of SGC.

Operation of SGC	Real number addition times	Real number multiplication times	Decision or comparison times
Normalization	N	N	0
Quantization	0	0	NN_0
Graph Construction	0	0	$N(N-1)/2$

As indicated in **Table 1**, for a sample size N, the total computational complexity of SGC is up to $O(N^2)$. When N is large, the computational complexity increases rapidly. Consequently, we attempted to solve the problem of balancing the recognition performance and operating time cost by modifying the input fed to SGC, and developed novel graphical feature, i.e., SD, to classify the BPSK and QPSK signals.

3.2 Graphical characteristics analysis of SS

First, we analyzed SS and its graphical transformation characteristics.

Definition 3. SS: We define the observed signal in time domain as $x(n)$, and the power spectrum of the squared signal is given by

$$Y(k)=(|\mathrm{DFT}[x^2(n)]|)^2, k=0,1,...N-1. \quad (7)$$

The SS of BPSK/QPSK signals are plotted in **Fig. 3**. Here, the coding scheme of the BPSK signal is [1,1,1,1,1,0,0,1,1,0,1,0,1], and that of the QPSK signal is [0,1,2,3,1,3,1,3,1,3,2,1,0], with the sampling interval $\Delta t = 0.01$ μs, carrier frequency $f_0 = 20.76$ MHz, code width $T_c = 640$ ns, sample size $N = 1024$, initial phase $\theta = \pi/4$, and SNR = 2 dB.

It is evident that after squaring, a BPSK signal becomes a sine wave with a single frequency of $2f_0$. Accordingly, its spectrum is a line spectrum along with the random noise spectrum. However, after the squaration, a QPSK signal becomes the BPSK signal, and its spectrum consists of the mixture of the narrow-band spectra and the random noise spectrum [7].

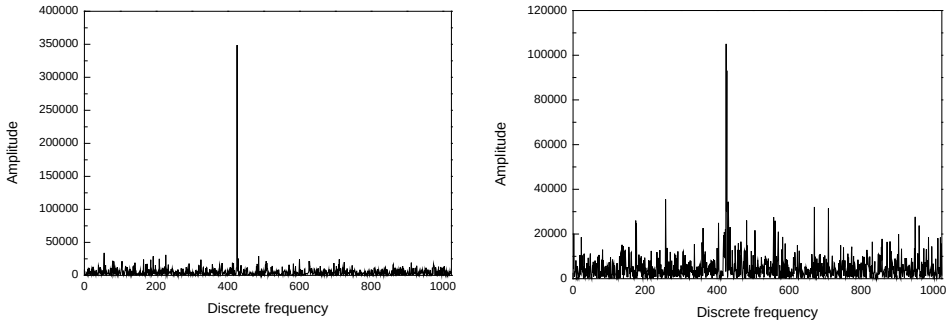

(a) (b)

Fig. 3. SS of modulation signals: (a) BPSK and (b) QPSK.

Definition 4. SD of a graph: For a simple undirected graph $G_Y(E_Y,V_Y)$, if its degree vector is denoted as $\mathbf{d}=(d_1,d_2,...,d_{N_0})^T$, then its SD is defined by $F=\sum_{i=1}^{N_0} d_i$.

Note that if the number of edges of the graph $G_Y(E_Y,V_Y)$ is defined as K, then SD can be expressed as $F=2K$. Thus, it can be deduced that SD is a linear function of the total number of edges of graph, and the relevant conclusions about the total number of edges of graph still apply to SD.

Proposition 1. (Schur–concavity of the expected number of total edges on the graph constructed from i.i.d. random sequences)

Considering an i.i.d. random sequence of sample size N that is converted into a simple undirected graph $G(E,V)$. The expected number of edges on the graph can be approximated by [14]

$$\varphi(\mathbf{p})=\sum_{\delta=1}^{N_0}\sum_{\beta=1}^{N_0}\left[1-\left(\frac{1}{p_\delta}\sum_{i=1,i\neq\beta}^{N_0}\omega_{\delta i}\right)^{p_\delta N}\right], \tag{8}$$

which is Schur–concave with respect to PVV $\mathbf{p}=(p_1,p_2,...,p_{N_0})^T$.

Proof. Let

$$\phi_\delta(\mathbf{p})=\sum_{\beta=1}^{N_0}\left[1-\left(\frac{1}{p_\delta}\sum_{i=1,i\neq\beta}^{N_0}\omega_{\delta i}\right)^{p_\delta N}\right], \delta=1,2,...,N_0 \tag{9}$$

,

equation (8) can be rewritten as

$$\varphi(\mathbf{p})=\sum_{\delta=1}^{N_0}\phi_\delta(\mathbf{p})=h[\phi_1(\mathbf{p}),\phi_2(\mathbf{p}),...,\phi_{N_0}(\mathbf{p})]. \tag{10}$$

According to the Proposition B .1 in [20] (Ch. 3. Page 88-89), if $\phi_\delta(\mathbf{p})$, $\delta=1,2,...,N_0$ is Schur–concave and $h(\phi)=\sum_{\delta=1}^{N_0}\phi_\delta$ represents an increase on $\mathbb{R}^N$, then $\varphi(\mathbf{p})$ is Schur–concave. Subsequently, equation (9) can be further rewritten as

$$\phi_\delta(\mathbf{p})=\sum_{\beta=1}^{N_0}\left\{1-\left[\frac{1}{p_\delta}\left(\sum_{i=1}^{N_0}\omega_{\delta i}-\omega_{\delta\beta}\right)\right]^{p_\delta N}\right\}=\sum_{\beta=1}^{N_0}\left\{1-\left[\left(\sum_{i=1}^{N_0}p_i-p_\beta\right)\right]^{p_\delta N}\right\}=\sum_{\beta=1}^{N_0}[1-(1-p_\beta)^{p_\delta N}] \tag{11}$$

Its first order derivate can be derived as

$$\frac{\partial\phi_\delta(\mathbf{p})}{\partial p_\beta}=\sum_{\beta=1}^{N_0}\frac{\partial[1-(1-p_\beta)^{p_\delta N}]}{\partial p_\beta}=p_\delta N(1-p_\beta)^{p_\delta N-1},\delta=1,\ldots,N_0. \tag{12}$$

Accordingly, it follows that

$$\begin{aligned}&(p_1-p_2)\left(\frac{\partial\phi_\delta}{\partial p_1}-\frac{\partial\phi_\delta}{\partial p_2}\right)\\&=(p_1-p_2)p_\delta N[(1-p_1)^{p_\delta N-1}-(1-p_2)^{p_\delta N-1}]\le 0.\end{aligned} \tag{13}$$

Because the function ϕ_δ is symmetric and differentiable with respect to $p_i, i=1,\ldots,N_0$ and (13) is not greater than zero, the function ϕ_δ is Schur–concave [20, 21], which means that $\varphi(\mathbf{p})$ is Schur–concavity.

Remark: Proposition 1 implies that for an i.i.d. random sequences to be converted into simple graphs with a specific number of the vertices, the total number of edges of the graphs increases with the increasing of randomness of PVV. Consequently, for two random sequences drawn from different distributions, with the same sample size and the number of the vertices, the randomness of the PVV determines the connectivity of the generated graph, i.e., determines the value of the SD. The more random the PVV is, the denser the connectivity of the generated graph is, and the larger the corresponding SD value is.

The partial sums under the two hypotheses are plotted in **Fig. 4**. Here, the numbers of the vertices on graphs are set as $N_0=10$. It can be observed that the inequality $S_{p_\Omega}>S_{q_\Omega}$ holds, indicating that the PVV $\mathbf{q}$ is majorized by $\mathbf{p}$; thus, $\mathbf{q}$ is more random than $\mathbf{p}$. In particular, the connectivity of the constructed graph under H_1 is greater than that under H_0 because $\mathbf{q}\prec\mathbf{p}$. Accordingly, the total number of edges of the graph constructed under H_1 is more than that under H_0. It can be utilized as a discriminate feature to differentiate BPSK and QPSK signals.

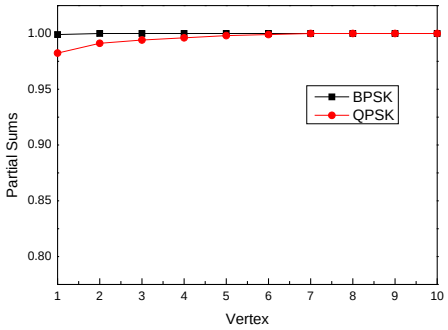

Fig. 4. Partial sums of PVVs for BPSK and QPSK signals.

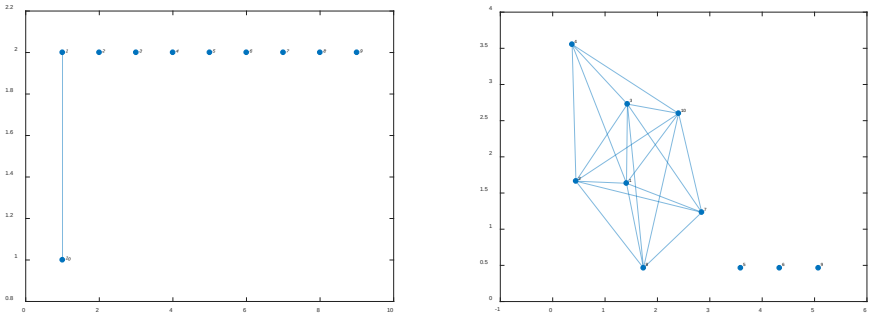

(a) (b)

Fig. 5. Graphs constructed from SSs of (a) BPSK and (b) QPSK signals.

Fig. 5 illustrates the graphs constructed from SSs of BPSK and QPSK signals. It can be observed that the graph generated from a BPSK signal is an isolated graph with SD of 2, whereas that generated from a QPSK signal is a giant connected graph with the SD of 38. This reveals a distinct difference between the two graphs in terms of connectivity. The phenomenon verifies the above-mentioned conclusion, where the randomness of the PVV determinates the connectivity of the generated graphs.

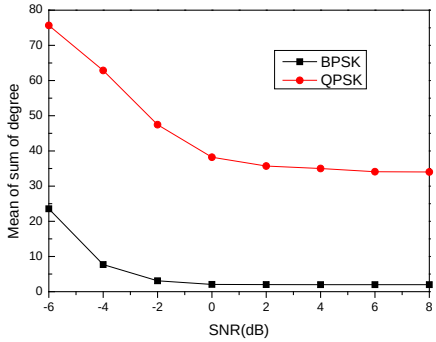

Fig. 6. Means of SD under two hypotheses.

Fig. 6 shows means of SDs under the two hypotheses versus SNR, where 1000 trials simulations were performed under each hypothesis. It can be observed from the figure that the average SDs under the two hypotheses differ distinctly. For H_0, the range of the average SD varies from 2 to 25, whereas for H_1, it varies from 35 to 75. In addition, with the increase of SNR, the average SD decreases and approaches a fixed value. It is because with the same SNR, the PVV under H_1 is more random than that under H_0; thus, the average SD value under H_1 is significantly greater than that under H_0.

3.3 Influence of TSS on connectivity of the graph

In this study, the necessary preprocessing was conducted before the SGC, including the calculation of the TSS. The purpose of calculating SS is to convert BPSK and QPSK signals into single frequency sine waves and BPSK signals, respectively. This technique can provide a basis for extracting more separable and stable features in the graph-based classification algorithm. In addition, the truncation operation can reduce the length of the samples fed to the

SGC, thereby reducing the computational complexity. In this case, the computational complexity is $O(D^2)$, where D denotes the length of the truncated signals ($D << N$). Similarly, when the original SS is used to construct a graph, the computational complexity is $O(N^2)$, which results in more operating time than $O(D^2)$.

Definition 5. TSS: We define the TSS as

$$Y_{TSS}(k)=\begin{cases}Y(k), 0\le k_{\max}-\dfrac{D}{2}\le k\le k_{\max}+\dfrac{D}{2}\le N-1\\ 0, \quad otherwise\end{cases}, \tag{14}$$

where $k_{\max}$ represents the position of the peak of $Y(k)$. In particular, the truncation is equivalent to adding a rectangular window on SS.

Subsequently, the influence of the graphical connectivity on the truncation will be evaluated via simulations and the majorization theory. **Fig. 7** presents the TSS under two hypotheses, where the window width $D=100$. Evidently, the main lobe of the SS is reserved after truncation. In particular, TSS of the BPSK signal contains nearly one large line spectrum, whereas that for QPSK contains several large line spectra in the bandwidth.

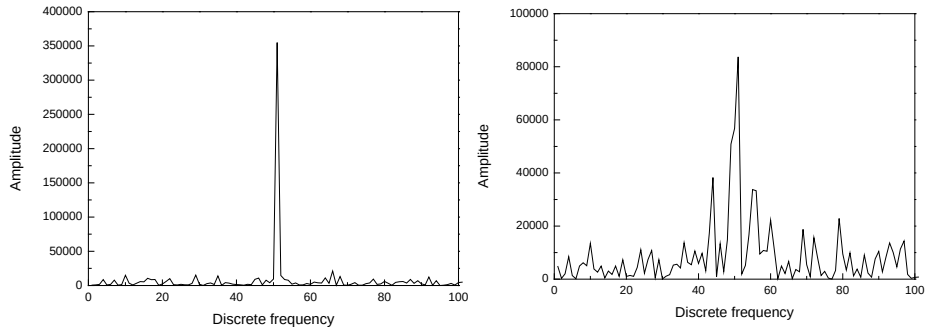

(a) (b)

Fig. 7. TSS of (a) BPSK and (b) QPSK.

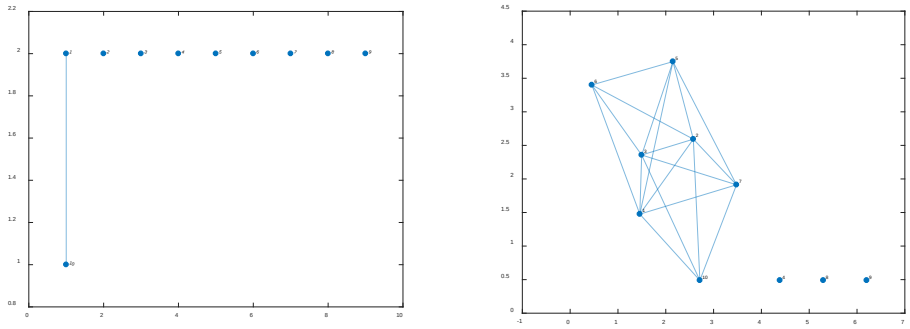

(a) (b)

Fig. 8. Graphs generated from TSS of (a) BPSK and (b) QPSK.

Fig. 8 illustrates the graphs generated from the TSS of BPSK and QPSK signals. It can be observed that under the two hypotheses, the graph structure retains its natural characteristics, which is similar to those in **Fig. 5**.

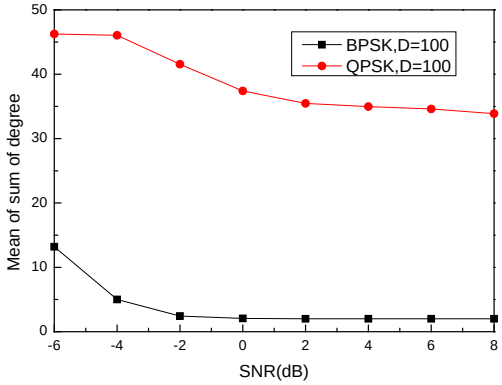

Fig. 9. Means of the SDs of the graphs constructed from TSS.

Fig. 9 depicts the average SDs of the graphs constructed from TSS. In total, 1000 trials were performed for each SNR. Notably, there are still significant differences in the average SDs under the two hypotheses. With the increase of SNR, the average SDs both decrease, and then gradually become fixed values.

The aforementioned phenomenon can be explained by the majorization relationship of the partial sum of the PVV after truncation under the two hypotheses. The partial sums of the PVV after truncation under the two hypotheses are plotted in **Fig. 10**. the truncation of the SS does not change the majorization relationship of the PVV under two hypotheses, and the SD feature of TSS can be used to classify BPSK and QPSK modulation signals with a low computational cost.

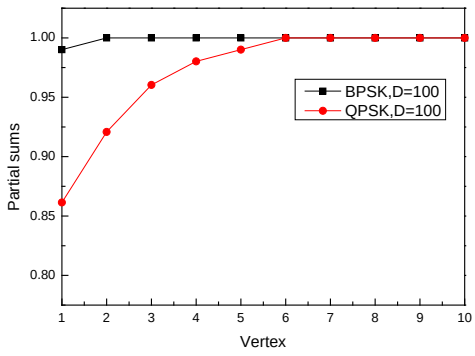

Fig. 10. Partial sums of PVV from TSS.

3.4 Summary of the proposed algorithm

The summary of the proposed algorithm is described in detail as follows.

Algorithm 1: BPSK/QPSK recognition algorithm based on TSS and SD

Input: Original observed signal $x(n)$, length of the rectangular window D, number of the vertices of a graph N_0, and threshold λ.

Output: recognition result.

Procedure:

1) Calculate SS $Y(k)$ by using (7);

2) Obtain truncated sequence $Y_{TSS}(k)$ by using (14);

3) Convert $Y_{TSS}(k)$ to graph $G_Y(E_Y, V_Y)$ with N_0 vertices by SGC;

4) Compute SD F of $G_Y(E_Y, V_Y)$;

5)Determine the modulation type of the signal $x(n)$ by comparing F with the threshold λ as follows: if $F < \lambda$, BPSK is chosen; else, QPSK is chosen.

Table 2. Computational complexity of the proposed algorithm.

Main operations	Real number addition times	Real number multiplication times	Decision or comparison times
Computation of SS	$N + 3N\log_2 N$	$3N + 2N\log_2 N$	0
SGC processing	D	D	$DN_0 + D(D-1)/2$

Regarding the computational complexity of the proposed algorithm, its principal operations include computation of SS and SGC. The computational complexity is listed in **Table 2**. According to the table, the total algorithm complexity is the order of $O(N + N\log_2^N + DN_0 + D^2)$.

4. SIMULATION RESULTS

4.1 Simulation setup

In this section, the proposed signal recognition scheme is evaluated via Monte Carlo simulations. Unless otherwise stated, the parameters used in the simulation are set as follows. The coding scheme of the BPSK signal is [1,1,1,1,1,0,0,1,1,0,1,0,1], and that of the QPSK signal is [0,1,2,3,1,3,1,3,1,3,2,1,0], with the sampling interval $\Delta t = 0.01\,\mu s$, carrier frequency $f_0 = 20.76$ MHz, code width $T_c = 640$ ns, sample size $N = 1024$, and initial phase $\theta = \pi/4$. The SNR was defined as $10\log_{10} A^2/(2\sigma^2)$ in dB, the number of the vertices on the constructed graph is $N_0 = 10$, window width is $D = 100$, and the predefined threshold $\lambda = 10$. In total, we performed 1000 trials for each condition under the two hypotheses.

4.2 Performance Evaluation

Fig. 11 shows the recognition accuracy of BPSK / QPSK signals under different SNRs. When the SNR is greater than or equal to -4 dB, the recognition accuracy of the BPSK signal exceeds 95%. However, the recognition accuracy of the QPSK signal is typically maintained at a rate of 100% within the range of SNRs selected. The result can be explained as follows. When the SNR is high, the distance between the SD features under the two hypotheses are consistently distinct and the recognition performance approaches 100%. However, when the SNR

decreases, even though the distance of the SD enlarges, its variance also becomes larger, which results in a decline in performance.

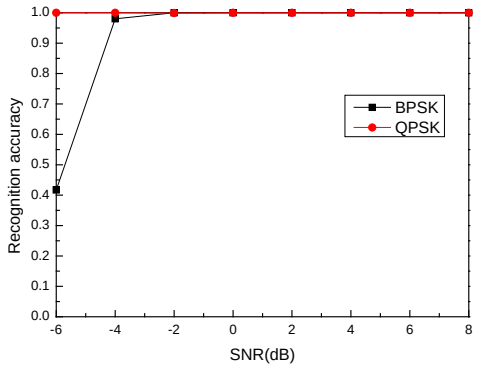

Fig. 11. Recognition performance of the proposed algorithm under different SNRs.

4.3 Effect of the sample size

Fig. 12 presents the average recognition accuracy of the proposed algorithm under different sample sizes. When the SNR is lower, for the same SNR, the average recognition accuracy increases with an increase in the sample size. When the SNR reaches -2 dB, the average recognition accuracies are close to 100%. The result can be explained as follows. Generally, an increase in the sample size of the signal in the time domain is equivalent to an increase in the SNR of TSS, provided that the points of the FFT are set as the sample size.

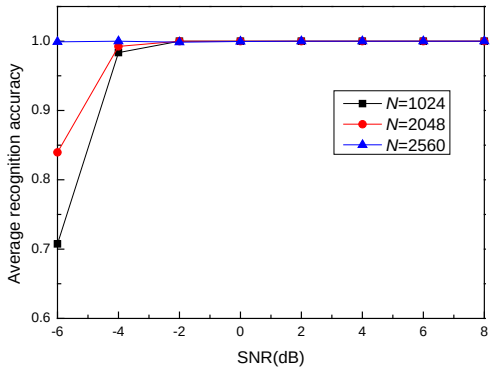

Fig. 12. Recognition performance of the proposed algorithm under different sample **sizes.**

4.4 Effect of initial phase

Fig. 13 depicts the average recognition accuracy of the proposed algorithm under different initial phase conditions. It can be observed that the change of the initial phase of the signal has no effect on the average recognition accuracy, primarily because the SS or TSS of BPSK / QPSK signal is the magnitude of the spectrum, and is unrelated to the initial phase.

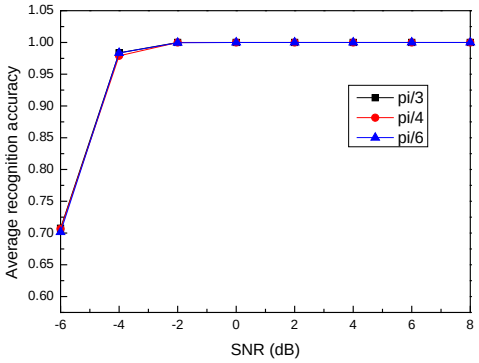

Fig. 13. Recognition performance of the proposed algorithm under different initial phases

4.5 Effect of window width

Fig. 14 shows the average recognition accuracy of the proposed algorithm under different window widths used in the truncation. It can be observed from the figure that the significantly smaller widths result in reducing the recognition performance. A small window width results in the loss of some important spectrum components of SS and disables the SD feature, which makes it unable to discriminate the modulation types. In contrast, a significantly large window causes high computational costs. However, if a moderate window length is selected: for example, greater than 25, the performance is robust when the SNR is greater than -4 dB. Hence, the width of the window selected in truncation should be moderated by concisely balancing the recognition performance and computational complexity.

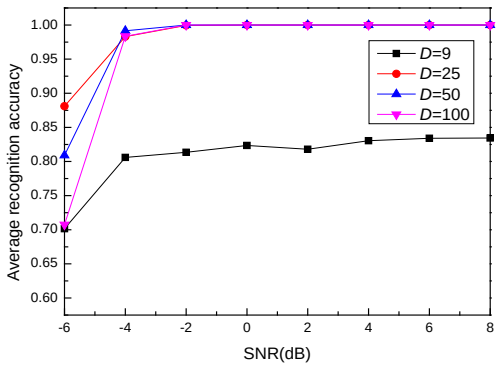

Fig. 14. Recognition performance of the proposed algorithm under different window widths.

4.6 Effect of the number of vertices on the graphs

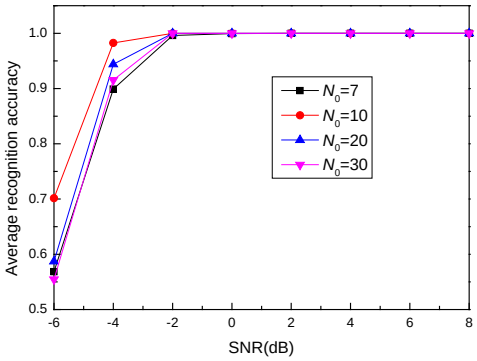

Fig. 15. Recognition performance of the proposed algorithm under different numbers of vertices.

Fig. 15 depicts the function between the number of vertices and recognition performance. On the one hand, it can be observed that when the SNR is high: for example, SNR>-2 dB, the performance is almost independent of the number of vertices. To be more specific, in such cases, the SD of the graph under two hypotheses are both with a lower variance, and have a distinct distance between each other. On the other hand, when the SNR is lower than -2 dB, a moderate number of vertices has optimal performance. A plausible explanation is that a significantly small or large numbers of vertices decrease or increase the value of the SD under the two hypotheses, respectively. Moreover, the distinguishability of features further decreases when combined with the influence of noise, thereby deteriorating the performance under an inadequate number of vertices.

4.7 Performance comparison with existing methods

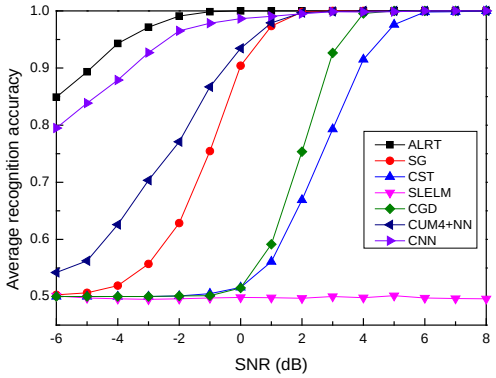

Fig. 16. Recognition performance comparisons between the proposed algorithm and the existing algorithms under different SNRs.

Fig. 16 illustrates the recognition performance comparisons among the proposed algorithm (denoted as SG), the second largest eigenvalue of Laplacian matrix-based algorithm in [15] (denoted as SLELM whose scheme is shown in Appendix), the complete graph detection-

based algorithm in [19] (denoted as CGD), the cyclostationary test-based algorithm in [7] (denoted as CST), the average likelihood ratio test algorithm in [22, 23] (denoted as ALRT), the forth order cumulant based on neural network algorithm in [22, 24] (denoted as CUM4+NN), and the convolutional neural network algorithm in [22, 25] (denoted as CNN). Here, the simulation conditions are set as those defined in section 2.2.6 in the literature [22]. For SG, the window width was set to 40. For SLELM, the number of modified points for SS was set to 7, and the number of vertices was set to 10. For CGD, the samples were normalized via Rayleigh distribution, and the number of vertices was set to 10. As expected, the ALRT algorithm exhibited the best performance. In general, the upper bound of the modulation recognition classification problem is obtained by the ALRT algorithm, which requires a priori information of the observed signal and accordingly has a limitation in practical contexts. Moreover, CNN-based and CUM4+NN-based algorithms perform better than the proposed algorithm. However, those algorithms severely depend on large amounts of training sets, concise SNR estimation, and matching operations, which are difficult in non-cooperative signal processing contexts. Importantly, the proposed algorithm is superior to the other three algorithms that do not rely on training sets.

Table 3. Comparison of the operating times between the proposed algorithm and existing algorithms.

Operating times (ms)	SLELM	CGD	SG	CST	ALRT	CNN	CUM4+NN
Training times	-	-	-	-	-	29148	54930
Testing times	6.14	9.02	5.65	8.37	7.33	0.76	0.27
Total times	6.14	9.02	5.65	8.37	7.33	29148.76	54930.27

Table 3 lists the average operating time comparisons between the proposed algorithm and other existing algorithms by conducting a complete identification trail. The hardware platform used in the simulation trial Included an Intel (R) core (TM) i7-8550u CPU (1.80GHz) processor, and MATLAB R2021a was used as a software platform to develop and execute the simulations. It can be observed that under identical conditions, if the training process is considered, the operation times of the algorithms based on NN or CNN are much higher than those of other algorithms. Among SLELM, CGD, SG, CST, and ALRT algorithms, the proposed algorithm has the shortest operation time. Considering the two vital factors of recognition performance and operation time, the proposed algorithm has much higher application value in situations where there is a lack of training samples, and a prior information of the signals and channels. Moreover, it is required for high real-time processing. In general, the proposed algorithm enhances the recognition performance of the graph-based algorithms, which is beneficial to extending the application for graph-based signal processing.

5 Conclusions

An innovative graph-based modulation classification of BPSK and QPSK signals is proposed in this study. TSS is utilized as an input fed to the SGC to construct an indirect graph. Subsequently, the SD of the graph is extracted as a classification feature to distinguish the modulation signals. In this study, large energy line spectrum was reserved by introducing TSS, which results in enhancing the processing SNR of the input fed to the SGC while reducing the computational complexity of signal-to-graph transformation. Simulation results indicated that compared with existing algorithms, the proposed algorithm achieves a satisfactory recognition

performance in lower SNRs without requiring any prior information of the signal and noise. As this method improves the efficiencies and recognition accuracies of existing graph-based algorithms, it can be applied in signal identification contexts that requiring real-time processing. However, the proposed algorithm has several limitations: for instance, the selection for the number of the vertices on graphs cannot be obtained analytically. In the future, we will attempt to develop new modulation recognition algorithms by combining the graph signal representation and deep learning framework to enhance the performance, which can be used in the context of multi-class signal classification, when the training samples are easy to obtain.

Appendix

SLELM Algorithm inspired by [15] is given below.

SLELM Algorithm : BPSK/QPSK recognition algorithm based on second largest eigenvalue of graph

Input: the original observed signal $x(n)$, vertices number of graph N_0, correction points M, and threshold λ_0.

Output: recognition result.

Procedure:

1) Calculate SS $Y(k)$ using (7);

2) Obtain the MSS using

$$Y_0(k)=\begin{cases}0, & k_{\max}-\dfrac{M}{2}\le k\le k_{\max}+\dfrac{M}{2}\\ X(k), & \text{otherwise}\end{cases},$$

where $k_{\max}$ represents the position of the peak of $Y(k)$.

3) Convert $Y_0(k)$ to a graph $G_{Y_0}(E_{Y_0},V_{Y_0})$ with N_0 vertices;

4) Compute the second largest eigenvalue of the Laplacian matrix of graph $G_{Y_0}(E_{Y_0},V_{Y_0})$, which is denoted by F_0;

5) Classify the signals $x(n)$ by comparing F_0 with the threshold λ_0, as follows:

if $F_0<\lambda_0$, BPSK is chosen; else, QPSK is chosen.

References

[1] O. A. Dobre, A. Abdi, Y. Bar-Ness, and W. Su, "Survey of automatic modulation classification techniques: classical approaches and new trends," *IET Communications*, vol. 1, no. 2, pp. 137-156, 2007. Article(CrossRef Link).

[2] Y. A. Eldemerdash, O. A. Dobre, and M. Öner, "Signal Identification for Multiple-Antenna Wireless Systems: Achievements and Challenges," *IEEE Communications Surveys & Tutorials*, vol. 18, no. 3, pp. 1524-1551, 2016. Article(CrossRef Link).

[3] T. J. O'Shea, T. Roy, T. C. Clancy, "Over-the-Air Deep Learning Based Radio Signal Classification," *IEEE Journal of Selected Topics in Signal Processing*, vol. 12, no. 1, pp. 168-179, 2018. Article(CrossRef Link).
[4] J. H., Peng S , Wang H , et al, " Modulation Classification Based on Signal Constellation Diagrams and Deep Learning," *IEEE Transactions on Neural Networks and Learning Systems*, vol. 30, no. 3, pp. 718-727, 2019. Article(CrossRef Link).
[5] J. W. Mendis G J , Madanayake A, "Deep learning-based automated modulation classification for cognitive radio," in *Proc. of IEEE International Conference on Communication Systems (ICCS)*, 2016. Article(CrossRef Link).
[6] P. C., F Meng, L Wu, et al, "Automatic Modulation Classification: A Deep Learning Enabled Approach," *IEEE Transactions on Vehicular Technology*, vol. 67, no. 11, pp. 10760-10772, 2018. Article(CrossRef Link).
[7] J. Reichert, "Automatic classification of communication signals using higher order statistics," in *Proc. of Acoustics, Speech, and Signal Processing, IEEE International Conference on*, vol. 5, pp. 221-224, 1992. Article(CrossRef Link).
[8] M. Ma, Z. Li, Y. Lin, L. Chen, and S. Wang, "Modulation Classification Method based on Deep Learning under Non-Gaussian Noise," in *Proc. of 2020 IEEE 91st Vehicular Technology Conference (VTC2020-Spring)*, 2020. Article(CrossRef Link).
[9] Y. Tu, Y. Lin, C. Hou, and S. Mao, "Complex-Valued Networks for Automatic Modulation Classification," *IEEE Transactions on Vehicular Technology*, vol. 69, no. 9, pp. 10085-10089, 2020. Article(CrossRef Link).
[10] Y. Dong, X. Jiang, H. Zhou, Y. Lin, and Q. Shi, "SR2CNN: Zero-Shot Learning for Signal Recognition," *IEEE Transactions on Signal Processing*, vol. 69, pp. 2316-2329, 2021. Article(CrossRef Link).
[11] J. Bai, L. Gao, J. Gao, H. Li, R. Zhang, and Y. Lu, "A new radar signal modulation recognition algorithm based on time-frequency transform," in *Proc. of 2019 IEEE 4th International Conference on Signal and Image Processing (ICSIP)*, pp. 21-25, 2019. Article(CrossRef Link).
[12] H.-C. Wu, M. Saquib, and Z. Yun, "Novel automatic modulation classification using cumulant features for communications via multipath channels," *IEEE Transactions on Wireless Communications*, vol. 7, no. 8, pp. 3098-3105, 2008. Article(CrossRef Link).
[13] F. Wang and X. Wang, "Fast and robust modulation classification via Kolmogorov-Smirnov test," *IEEE Transactions on Communications*, vol. 58, no. 8, pp. 2324-2332, 2010. Article(CrossRef Link).
[14] W. H. C., Yan K , Busch C , et al, "Graph representation of random signal and its application for sparse signal detection," *Digital Signal Processing*, vol. 96, p. 102586, 2020. Article(CrossRef Link).
[15] W. H. C. Yan K , Xiao H , et al, "Novel Robust Band-Limited Signal Detection Approach Using Graphs," *IEEE Communications Letters*, vol. 21, no. 1, pp. 20-23, 2017. Article(CrossRef Link).
[16] X. Yan, G. Liu, H.-C. Wu, G. Zhang, Q. Wang, and Y. Wu, "Robust modulation classification over α-stable noise using graph-based fractional lower-order cyclic spectrum analysis," *IEEE Transactions on Vehicular Technology*, vol. 69, no. 3, pp. 2836-2849, 2020. Article(CrossRef Link).
[17] X. Yan, G. Liu, H.-C. Wu, and G. Feng, "New automatic modulation classifier using cyclic-spectrum graphs with optimal training features," *IEEE Communications Letters*, vol. 22, no. 6, pp. 1204-1207, 2018. Article(CrossRef Link).
[18] X. Yan, G. Zhang, H.-C. Wu, and G. Liu, "Automatic modulation classification in α-stable noise using graph-based generalized second-order cyclic spectrum analysis," *Physical Communication*, vol. 37, pp. 100854-100962, 2019. Article(CrossRef Link).
[19] Y. A. Eldemerdash, O. A. Dobre, O. Üreten, and T. Yensen, "A Robust Modulation Classification Method for PSK Signals Using Random Graphs," *IEEE Transactions on Instrumentation and Measurement*, vol. 68, no. 2, pp. 642-644, 2019. Article(CrossRef Link).
[20] I. O. A. W. Marshall, *Inequalities: Theory of Majorization and Its Applications*, New York: Academic Pres, 1979.

[21] T. Nakata, "Coupon collector's problem with unlike probabilities," *Journal of Classical Analysis*, vol. 14, no. 2, pp. 177-180, 2019. Article(CrossRef Link).
[22] Z. Lei, "Research on Deep Learning Based Modulation Recognition Technologies, " University of Electronic Science and Technology of China, 2019.
[23] W. Wei and J. M. Mendel, "Maximum-likelihood classification for digital amplitude-phase modulations," *IEEE Transactions on Communications*, vol. 48, no. 2, pp. 189-193, 2000. Article(CrossRef Link).
[24] O. A. Dobre, A. Abdi, Y. Bar-Ness, and W. Su, "Selection combining for modulation recognition in fading channels," in *Proc. of Military Communications Conference*, pp. 2499-2505, 2005. Article(CrossRef Link).
[25] T. O'Shea, T. Roy, and T. C. Clancy, "Over-the-Air Deep Learning Based Radio Signal Classification," *IEEE Journal of Selected Topics in Signal Processing*, vol. 12, no. 1, pp. 168-179, 2018. Article(CrossRef Link).

Li Yang received the M.S. degree in signal and information processing from Yangzhou University, China, in 2008. Currently, she is a senior experimentalist at College of Electronic and Information Engineering, Jinling Institute of Technology. Her main research interests include radar signal detection & recognition.

Guobing Hu received the M.S. and Ph.D. degrees in electronic and information engineering from Nanjing University of Aeronautics and Astronautics, China, in 2006 and 2011, respectively. Currently, he is a Professor in the Department of Electronics and Information Engineering, Jinling Institute of Technology, and is a visiting scholar at Southeast University. His main research interests are radar signal processing and digital signal processing, with a particular focus on non-cooperative communications, cognitive radio systems, and multiple-input multiple-output antenna systems.

Xiaoyang Xu received the M.S. degree in signal and information processing from Nanjing University of Posts and Telecommunications, China, in 2012. Currently, she is an experimentalist at College of Network Communication Engineering, Jinling Institute of Technology, China. Her main research interest includes radar signal processing.

Pinjiao Zhao received the B.S. and Ph.D. degrees in Electronic and Information Engineering and Information and Communication Engineering from Harbin Engineering University, China, in 2013 and 2017, respectively. Currently, she is an associate professor at College of Electronic and Information Engineering, Jinling Institute of Technology, China. Her main research interests include radar signal processing and high precision passive direction finding.